Regulation of magnon-phonon coupling by phonon angular momentum in two-dimensional systems

Qian Wang ![ORCID], Shuang Liu, Meng-Qiu Long,[*] and Yun-Peng Wang[†]

Hunan Key Laboratory for Super-Microstructure and Ultrafast Process, School of Physics,
Central South University, 932 South Lushan Road, Changsha 410000, People's Republic of China

The coupling between magnons and phonons modulates the transport properties of magnons, resulting in magnon polarons and magnon Seebeck effects, etc. Magnons possess well-defined angular momentum, while phonons are usually composed of linear atomic oscillations lacking angular momentum. However, in chiral systems, phonons become elliptical or circular; thus they will carry angular momentum. In this paper, we emphasize angular momentum and its role in the magnon-phonon coupling. Using a coupled-magnon-phonon model on the hexagonal lattice, we investigate the coupling of achiral and chiral phonons with three types of magnons, namely a magnon on one sublattice, ferromagnetic magnons, and antiferromagnetic magnons. We calculate the magnon-phonon dispersion relations and the strength of magnon-phonon coupling in the reciprocal space. We are particularly interested in the K and K' points at the corner of the first Brillouin zone where the normal modes involve circular rotations of magnetization and displacement. We find a selective coupling wherein the coupling between magnons and phonons vanishes either when the magnitude of the magnon or phonon modes is zero or when the circular motion of magnetization is opposite to that of the displacements. These findings pave the way towards manipulating magnon polaron devices based on phonon angular momentum.

I. INTRODUCTION

Both magnons and phonons are bosonic collective excitations in magnetic materials. When they are in the resonant condition with coincidence in both their wavelength and frequency, the precession of the magnetic moments stimulates the vibration of the lattice, and the lattice vibration also excites the spin wave, which results in magnon-phonon coupling [1–3]. The magnon-phonon coupling is usually characterized by the avoided crossing in their energy dispersions. When the magnon-phonon coupling strength is larger than the lifetimes of magnons and phonons, the coupled magnon and phonon form a composite quasiparticle dubbed the magnon polaron [4–6]. The large Berry curvature within the avoided crossing region contributes to the thermal Hall effect [6–9], which provides a routine to tune the thermal and spin currents in magnetic materials. Magnetoacoustic coupling gives the nontrivial topological properties of the magnon, which play an important role in magnon transport characteristics, such as the spin Nernst effect [10] and spin Seebeck effect [11].

Magnons possess quantized spin angular momentum. The interaction between magnons and phonons has been discussed from the perspective of angular momentum. The relaxation process of a single magnetic moment within a lattice shall conserve the total angular momentum [12], and so do the interactions between magnons and phonons [13]. Mutual conversion between magnons and phonons is accompanied by the angular momentum transfer between lattice and spin [8,14–16].

Phonons were also demonstrated to carry intrinsic angular momentum in chiral systems. The angular momentum of phonons is associated with rotations of atoms around their equilibrium positions. Chiral phonons, proposed by Zhang and co-workers [17–19], exist in inversion-symmetry-broken systems, such as triangular [20], Kekulé [21], honeycomb [22], and kagome lattices [23]. Inversion symmetry in the hexagonal lattice can be broken by isotopic doping and a staggered sublattice potential [24,25]. Phonons can also acquire angular momentum through coupling with the magnetism in time-reversal-symmetry-breaking systems [18]. Time-reversal symmetry can be broken by an external magnetic field [1,26,27] or Coriolis force in rotating systems [28–30]. The dispersion relation of magnons and phonons in chiral systems is nonreciprocal [31], and this is attributed to magnon-phonon coupling.

Magnon-phonon coupling has been observed in two-dimensional (2D) magnetic materials, including FePS$_3$ [32], FePSe$_3$ [33], and CrI$_3$ [34]. Magnon-phonon coupling in a honeycomb lattice has been theoretically studied [6]. Zhang and Niu [17] demonstrated the existence of chiral phonons with quantized pseudoangular momentum in the honeycomb lattice. In this paper, we study the magnon coupling with achiral and chiral phonons in a honeycomb lattice, especially the role played by phonon angular momentum in determining the magnon-phonon coupling strength. Our results demonstrate a selective magnon-phonon coupling that vanishes at some high-symmetry points. The results are analyzed in terms of the phonon angular momentum of each sublattice, instead of the total phonon angular momentum.

---
[*]mqlong@csu.edu.cn
[†]yunpengwang@csu.edu.cn

The remainder of this paper is organized as follows. Our calculation method is presented in Sec. II. Combining the Landau-Lifshitz equation [35,36] and Newton's second law, we derive the equations of motion (EOMs) for coupled magnons and phonons, which serve as a unified theoretical framework to describe the motion of atoms and the precession of magnetic moments in magnetic insulators. In Sec. III, we discuss the results for three types of honeycomb lattices, namely (1) a honeycomb lattice in which only one sublattice is magnetic, (2) a honeycomb lattice in which two magnetic sublattices are in the ferromagnetic state, and (3) a honeycomb lattice in which two magnetic sublattices are in the antiferromagnetic state. The vanishing magnon-phonon coupling at high-symmetry points is analyzed based on the phonon polarization of sublattices. Our conclusions are given in Sec. IV.

II. METHODS

A. Equations of motion

Consider a magnetic insulator possessing both lattice vibrations and spin waves simultaneously. The motion of atoms is described by Newton's second law; we take the Landau-Lifshitz equation [35,36] to describe the precession of local magnetic moments. The former is a second-order differential equation, while the latter is first order; their different orders prevent unified equations of motion for both lattice and spin dynamics. Alternatively, one can take both the displacements and velocities of atoms as variables, which decomposes Newton's equation into two first-order differential equations. The equations of motion for magnons and phonons have been derived in our previous work [37]. In this paper, we rewrite the equations of motion in a matrix form; therefore the dispersion relation can be easily solved by diagonalizing the corresponding dynamic matrix. The state of a coupled spin-lattice system is characterized by three vector variables: the velocity of atoms (dubbed V), the displacement of atoms from their equilibrium positions (U), and the deviation of local magnetic moments from their equilibrium directions (S). The equations of lattice and spin motions are a first-order differential equation of these variables.

Forces on atom j (F_j) and the effective local magnetic field (B_j) can be calculated from the derivative of the total energy H with respect to U_j and S_j. That is, $F_j = -\partial H/\partial U_j$, $B_j = -\partial H/\partial S_j$. It is the torque on a local magnetic moment that determines its dynamics, which is defined as $T_j = \gamma h_j \times S_j$, where γ is the gyromagnetic ratio.

The equations of motion for V, U, and S (omitting their dependence on the time t and their atomic index j) can be expressed as

$$\frac{d}{dt}\begin{pmatrix} V \\ U \\ S \end{pmatrix} = \begin{pmatrix} F/m \\ V \\ T \end{pmatrix} = \begin{pmatrix} 0 & D & A \\ 1 & 0 & 0 \\ 0 & B & C \end{pmatrix} \cdot \begin{pmatrix} V \\ U \\ S \end{pmatrix}, \quad (1)$$

where $D \equiv d(F/m)/dU$ and $C \equiv dT/dS$ describe the lattice interaction and the spin-spin interaction, respectively. The coupling between spin and lattice is represented by $A \equiv d(F/m)/dS$ and $B \equiv dT/dU$. The form of these matrix blocks is determined by the form of the total energy H; in practice, they are calculated using the finite difference

method in this paper. For example, when an atom moves in the $\pm x$ direction with a displacement of ΔU, we can get the energy difference ($H_{x_+} - H_{x_-}$) in the x direction. Using the finite difference, we can calculate the force on atoms along the x direction as $F_x = (H_{x_+} - H_{x_-})/(2\Delta U)$. Then, rotating the magnetic moment S in the $\pm x$ or $\pm y$ direction with a displacement of δS and using the finite difference, we can solve matrix A. Each element of matrix A can be represented as $A_{ij}^{\alpha\beta} = (F_i^\alpha - F_j^\beta)/(2\delta S)$. Here, i, j is the number of atoms, and α, β represent the direction of x, y, and z, respectively. In the same way, we can obtain matrices B, C, and D. So the big matrix on the right side in Eq. (1) is the dynamic matrix, which plays essentially the same role as the Hamiltonian in the Schrödinger equation. For a finite system, the frequencies of excitations multiplied by the imaginary number i are equal to the eigenvalues of the dynamic matrix.

For an extended crystal, one can take the Fourier transformation of Eq. (1). For a given k point, Eq. (1) becomes

$$\frac{d}{dt}\begin{bmatrix} V(t;\vec{k}) \\ U(t;\vec{k}) \\ S(t;\vec{k}) \end{bmatrix} = \begin{bmatrix} 0 & D(\vec{k}) & A(\vec{k}) \\ 1 & 0 & 0 \\ 0 & B(\vec{k}) & C(\vec{k}) \end{bmatrix} \cdot \begin{bmatrix} V(t;\vec{k}) \\ U(t;\vec{k}) \\ S(t;\vec{k}) \end{bmatrix}, \quad (2)$$

where the dependences on the time t and the k point are included.

We seek solutions in the form of

$$\begin{bmatrix} V(t;k) \\ U(t;k) \\ S(t;k) \end{bmatrix} = \begin{bmatrix} V_0(\vec{k}) \\ U_0(\vec{k}) \\ S_0(\vec{k}) \end{bmatrix} e^{i\omega t}, \quad (3)$$

which are the solutions of the eigenproblem of

$$\begin{bmatrix} 0 & D(\vec{k}) & A(\vec{k}) \\ 1 & 0 & 0 \\ 0 & B(\vec{k}) & C(\vec{k}) \end{bmatrix} \cdot \begin{bmatrix} V_0(\vec{k}) \\ U_0(\vec{k}) \\ S_0(\vec{k}) \end{bmatrix} = i\omega \begin{bmatrix} V_0(\vec{k}) \\ U_0(\vec{k}) \\ S_0(\vec{k}) \end{bmatrix}. \quad (4)$$

B. Sublattice polarizations of phonon modes

Chiral phonons are characterized by rotations of atoms around their equilibrium positions [17,23,38]. The displacement of one atom within the sublattice α can be written as

$$\vec{u}_\alpha(\vec{k}, \vec{R}, t) = C_\alpha \mathrm{Re}\big[e^{-i\vec{k}\cdot\vec{R}} e^{i\omega t} \vec{\epsilon}_\alpha(\vec{k})\big], \quad (5)$$

where C_α is the amplitude of displacement and $\vec{k}$ and ω are the phonon wave vector and frequency. $\vec{R}$ is the position of the unit cell where the atom resides. Suppose that the atom rotates around the z axis; $\vec{\epsilon}_\alpha(\vec{k})$ is a normalized two-component vector. Analogously to circularly polarized photons, one can decompose the polarization $\vec{\epsilon}_\alpha(\vec{k})$ into clockwise (CW) and counterclockwise (CCW) rotations,

$$\vec{\epsilon}_\alpha = \frac{a}{\sqrt{2}}\begin{pmatrix} 1 \\ i \end{pmatrix} + \frac{b}{\sqrt{2}}\begin{pmatrix} 1 \\ -i \end{pmatrix} \equiv a|R\rangle + b|L\rangle, \quad (6)$$

where the dependence on $\vec{k}$ is omitted for clarity. The state $|R\rangle$ corresponds to CCW rotation, while $|L\rangle$ is the CW rotation. One can define an operator $\hat{P}$, $|R\rangle$ is its eigenvector with eigenvalue of $+1$, and $|L\rangle$ is its eigenvector with eigenvalue

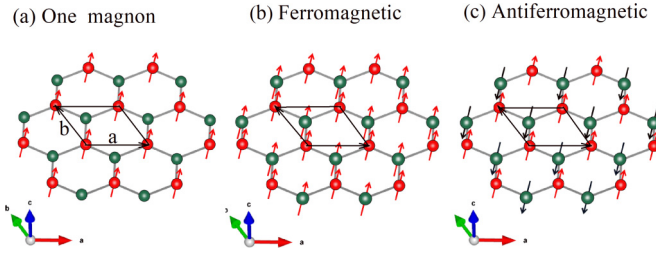(a) One magnon   (b) Ferromagnetic   (c) Antiferromagnetic

FIG. 1. Schematics of a honeycomb lattice with two atoms, atom A (red) and atom B (green): (a) one magnon, (b) ferromagnetic, and (c) antiferromagnetic. Here, "a" and "b" are the lattice vectors shown by black arrows. The interatomic bond length is 1, and the lattice constant is $\sqrt{3}$. The red arrows indicate the spin direction.

of -1,

$$\hat{P} = |R\rangle\langle R| - |L\rangle\langle L| = \begin{pmatrix} 0 & -i \\ i & 0 \end{pmatrix}. \tag{7}$$

One can then define the polarization of sublattice α as

$$P_\alpha^z = (\vec{\epsilon}_\alpha)^\dagger \hat{P} \vec{\epsilon}_\alpha, \tag{8}$$

which is a real number between -1 and $+1$. The CW circular rotation has a polarization of $P_\alpha^z = -1$, while the CCW circular rotation has a polarization of $P_\alpha^z = +1$. The linear motion with the atom moving back and forth along a line corresponds to $P_\alpha^z = 0$. Elliptic rotations have a noninteger polarization.

The sublattice polarization can be used to express the angular momentum of phonons, as discussed by Zhang and Niu [17]:

$$L_z = \sum_\alpha C_\alpha m_\alpha P_\alpha^z, \tag{9}$$

where m_α is the atomic mass of sublattice α and C_α is the amplitude of displacement.

III. RESULTS

In this paper, we focus on a magnetic insulator with local spins on a two-dimensional honeycomb lattice. We study the magnon-phonon coupling in three different systems as depicted in Fig. 1, namely a honeycomb lattice in which only one sublattice carries local spins while the other does not [Fig. 1(a)], a honeycomb lattice in which both sublattices are magnetic and they are ferromagnetically coupled [Fig. 1(b)], and a honeycomb lattice in which both sublattices are magnetic and they are antiferromagnetically coupled [Fig. 1(c)]. The total energy has three components,

$$H = H_m + H_p + H_c, \tag{10}$$

where H_m describes the coupling between local magnetic moments, H_p is the energy due to the lattice interactions, and H_c represents the magnon-phonon coupling.

The term H_m consists of isotropic Heisenberg interactions between localized magnetic moments,

$$H_m = -J \sum_{\langle ij \rangle} \vec{S}_i \cdot \vec{S}_j. \tag{11}$$

For the model shown in Fig. 1(a), H_m describes the magnetic interactions between nearest neighbors within the magnetic

sublattice. For the models in Figs. 1(b) and 1(c), H_m represents the magnetic interactions between different sublattices, $J > 0$ corresponds to the ferromagnetic (FM) state, and $J < 0$ is the antiferromagnetic (AFM) state.

The term H_p consists of kinetic and potential energies of the lattice,

$$H_p = \sum_j \frac{1}{2} m_j V_j^2 + \frac{k_1}{2} \sum_{\langle i<j \rangle} \left[(\vec{U}_i - \vec{U}_j) \cdot \hat{R}_{ij}^0 \right]^2$$
$$+ \frac{k_2}{2} \sum_{\langle i<j \rangle} \left[(\vec{U}_i - \vec{U}_j) \cdot \hat{R}_{ij}^0 \right]^2, \tag{12}$$

where m_j, $\vec{V}_j$, and $\vec{U}_j$ are the mass, velocity, and position of the jth atom and k_1 and k_2 are the spring constants for longitudinal and transverse distortions. The unit vector pointing from the equilibrium position of the atoms i to atom j is denoted as $\hat{R}_{ij}^0$.

The magnetic interactions depend on the instant position of magnetic ions. Within the linear spin wave theory, lattice modulations are caused by both the isotropic interaction and the Dzyaloshinskii-Moriya interaction (DMI) [39–41]. The DMI has in-plane and out-of-plane components. The out-of-plane component modifies the magnon dispersion relation. The in-plane component introduces coupling between the magnon and phonon. In this paper, we only consider the in-plane component with an in-plane DMI vector for studying the magnon-phonon coupling. We adopt the form given by Zhang *et al.* in Ref. [8] (see Kittel [42]). The in-plane DMI has the form of $D_\parallel(R_{ij}) = -D_\parallel \hat{z} \times \hat{R}_{ij}$. The magnon-phonon coupling term can be written as

$$H_c = -D_\parallel \sum_{ij} \hat{z} \times (\vec{U}_i - \vec{U}_j) \cdot (\vec{S}_i \times \vec{S}_j), \tag{13}$$

where the summation is taken within sublattices i and j. $D_\parallel$ is the coupling coefficient. The spin operator $\vec{S}_i$ can be described as $\vec{S}_i = S\hat{z} + \delta\vec{S}_i$, where $\delta\vec{S}_i$ are the fluctuations around spin operators $\vec{S}_i$.

A. Sublattice polarization of phonons

Before discussing the magnon-phonon coupling, we first analyze the polarization of phonons. The phonon dispersion relation and normal modes are calculated in Eq. (12). The honeycomb lattice shown in Fig. 1 consists of two nonequivalent atoms per primitive cell, dubbed atoms A (red) and B (green).

The case of equal mass. Setting atoms A and B with the same mass $m_A = m_B$, we computed the phonon normal modes by diagonalizing the dynamic matrix in Eq. (2). The phonon dispersion relation and the normal modes at the K and K' points within the home primitive cell are shown in Fig. 2. In other primitive cells, the normal mode has extra phase factors. Figures 2(i) and 2(j) show four phonon bands, where the other two bands involving out-of-plane vibrations have vanishing frequencies. The four bands are denoted as bands 1–4 according to their frequencies.

We first discuss the normal modes at the K point as shown in Figs. 2(a)–2(d). For the lowest acoustic band, band 1, its normal mode comprises the circular rotations of both atom A and atom B. The trajectories of the atoms correspond to the
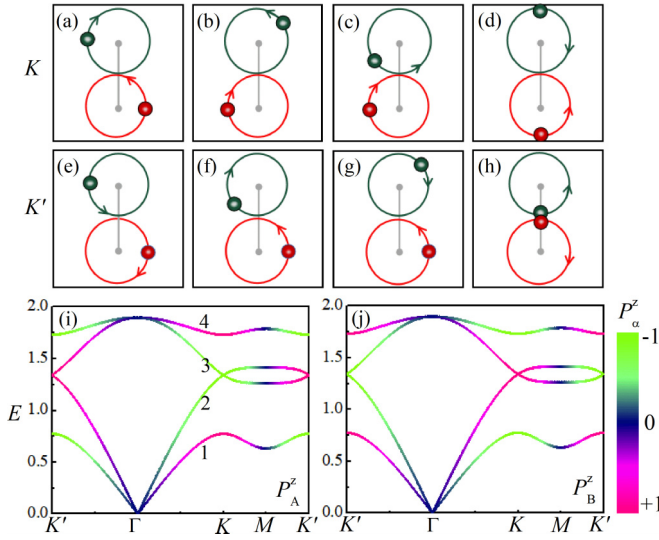
FIG. 2. Phonon vibration modes for atoms A and B in one honeycomb lattice with $m_A = m_B$. [(a)–(d)] The phonon modes for bands 1–4 at the K point, respectively. [(e)–(h)] The phonon modes for bands 1–4 at the K' point, respectively. (i) The phonon polarization of atom A. (j) The phonon polarization of atom B. In [(a)–(h)], atoms A and B are shown in red and green, respectively. In (i) and (j), the color indicates the direction of P_A^z and P_B^z, and the thickness of the curves represents the amplitudes C_A and C_B.
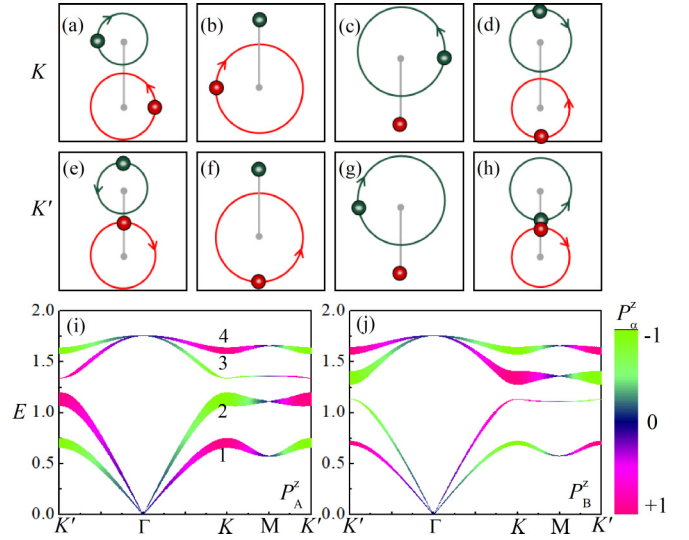

FIG. 3. Phonon vibration modes for atoms in one honeycomb lattice with $m_A = 1.4\,m_B$. [(a)–(d)] The phonon modes for bands 1–4 at the K point, respectively. [(e)–(h)] The phonon modes for bands 1–4 at the K' point, respectively. (i) The phonon polarization of atom A. (j) The phonon polarization of atom B. In [(a)–(h)], atoms A and B are shown in red and green, respectively. In (i) and (j), the color indicates the direction of P_A^z and P_B^z, and the thickness of the curves represents the amplitudes C_A and C_B.

red and green circles in Fig. 2(a), where the arrows stand for the direction of rotation and the spheres on the trajectories stand for the positions of the atoms at time $t = 0$. The rotations of atoms A and B have a phase difference of π. Atoms A and B rotate in opposite directions: For the normal mode at the K point, atom A rotates CCW while atom B rotates CW. The radius of the trajectory of atom A is equal to that of atom B ($C_A = C_B$). In addition, the normal modes of band 4 are the same as those of band 1, as shown in Fig. 2(d).

Bands 2 and 3 are degenerate at the K point. In the normal modes of bands 2 and 3, atoms rotate in an opposite pattern to that of bands 1 and 4; that is, atom A rotates CW while atom B rotates CCW [see Figs. 2(b) and 2(c)]. The rotations of atoms A and B have a phase difference of $3\pi/4$ and $\pi/4$ for bands 2 and 3, respectively. The normal modes at the K' point [Figs. 2(e)–2(h)] are related to those at the K point by time-reversal symmetry; that is, atoms move in the opposite direction compared with the normal mode at the K point. The phonon polarization of each sublattice P_α^z calculated using Eq. (8) is denoted by the pseudocolor in Figs. 2(i) and 2(j). The value of P_A^z is opposite to that of P_B^z at each point. As a result, the total angular momentum of the phonons defined as Eq. (9) vanishes.

The case of different masses. By setting different masses for atoms A and B, the inversion symmetry breaks, and the honeycomb lattice becomes chiral. We set $m_A = 1.4\,m_B$ in the calculations, and the results are shown in Fig. 3. The degeneracy at the K and K' points is lifted, and the dispersion relation is depicted in Figs. 3(i) and 3(j). Band 2 possesses a sublattice polarization of $P_A^z = -1$ (+1) at the K (K') point, while sublattice B is frozen at its equilibrium position with a displacement amplitude C_B of zero. The angular momentum

of band 2 at the K (K') point is solely contributed by sublattice A. Similarly, sublattice B is the only contributor to the angular momentum of band 3 at the K (K') point. The emergence of finite phonon angular momentum agrees with the findings of Zhang and Niu [17,18].

The normal modes shown in Figs. 3(a)–3(h) are also different from the normal modes in the case of equal mass in Fig. 2. The trajectories of atoms A and B no longer have the same radius. For bands 1 and 4, the trajectory of atom A has a larger radius than the trajectory of atom B. For band 2 at the K and K' points, the normal mode consists of a rotation of atom A, while atom B stays at its equilibrium position with $C_B = 0$; see Figs. 3(b) and 3(f). For band 3, only atom B moves. The calculated dispersion relation of phonons is shown in Figs. 3(i) and 3(j). The color in Fig. 3(i) represents the phonon polarization on sublattice A (P_A^z), and the color in Fig. 3(j) represents the phonon polarization on sublattice B (P_B^z); the thickness of the curves stands for the amplitudes C_A and C_B.

B. Magnon-phonon coupling

1. The case of only one magnetic sublattice

We first study the model shown in Fig. 1(a) with a magnetic sublattice A and a nonmagnetic sublattice B. In the ground state, local spins on sublattice A point to the $+z$ direction. The precession of local spins corresponds to a CCW rotation of the deviation of local spin S. The magnon-phonon dispersion is calculated by diagonalizing the dynamic matrix in Eq. (2). Figure 4(a) shows the case of $m_A = m_B$, where the pseudocolor stands for the weights of magnons and phonons in the normal modes. The red color corresponds to pure magnon,
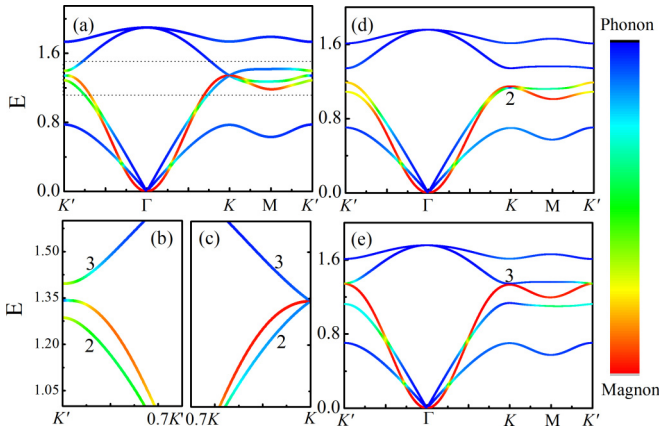
FIG. 4. Hybrid magnon-phonon modes in one magnetic ion. (a) Energy bands of magnon-phonon coupling with $J = 1.5$ and $m_A = m_B$. (b) Enlarged view near the K' point in (a). (c) Near the K point the enlarged view in (a). (d) The one magnon coupled with phonon band 2 with $m_A = 1.4 \, m_B$ and $J = 1.4$. (e) The magnon-phonon coupling in phonon band 3 with $m_A = 1.4 \, m_B$ and $J = 1.6$.
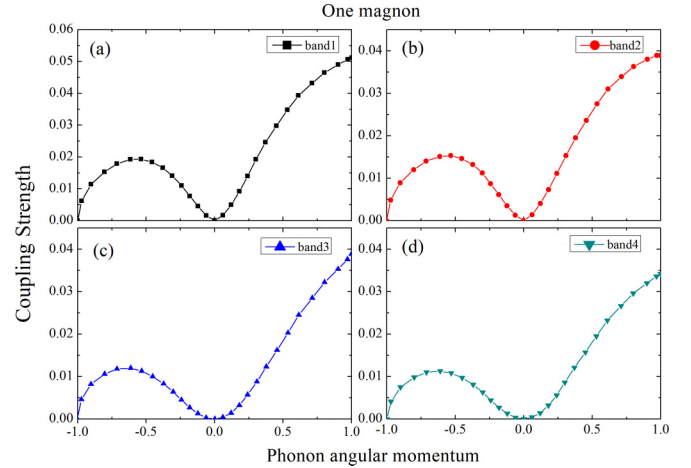

FIG. 5. The magnon-phonon interaction strengths as a function of phonon angular momentum. (a), (b), (c), and (d) The coupling of phonon bands 1, 2, 3, and 4 with the magnon, respectively.

while blue is for pure phonon. When a magnon band crosses a phonon band, they usually hybridize to form a magnon polaron, which is represented by the green color. As shown in Fig. 4(a), whenever the magnon band crosses a phonon band, their colors turn to green, indicating a hybridization between them. However, looking at the K point with an energy of about 1.35, the magnon band remains red, and the phonon band remains blue, as shown in Fig. 4(c). The phonon acoustic band (labeled as band 2) and the optical band (labeled as band 3) form a Dirac cone; there is no signature of band anticrossing. The magnon-phonon coupling vanishes at the K point. In contrast, at the K' point [see Fig. 4(b)], the magnon and phonon are strongly coupled: The green color means that these states have mixed magnon-phonon features. In addition, the Dirac cone formed by acoustic and optical phonon bands at the K' point disappears. There is a finite magnon-phonon coupling strength at the K' point. The magnon-phonon interaction strengths as a function of phonon angular momentum are shown in Fig. 5. Therefore we know that the coupling of magnons with phonons is selective.

The selective magnon-phonon coupling shall be attributed to the difference in the phonon modes at the K and K' points, since the magnon normal mode always consists of CCW rotation of spin on atom A with $S_A^z = +1$. As shown in Figs. 2(b) and 2(c), at the K point the normal mode of phonon bands 2 and 3 consists of CW rotation of atom A; so both bands are characterized by phonon polarization of sublattice A with $P_A^z = -1$. However, at the K' point, atom A in phonon bands 2 and 3 involves CCW rotation, and P_A^z is $+1$; see Figs. 2(f) and 2(g).

Recalling that the magnon couples with phonons at the K' point but not with phonons at the K point, we speculate that the phonon polarization of sublattice A determines the magnon-phonon coupling strength: The phonon mode with $P_A^z = +1$ is strongly coupled to the magnon of $S_A^z = +1$. Figures 4(d) and 4(e) show the calculated dispersion relation when the masses of atom A and atom B are different. We tune the magnetic exchange parameter J in Eq. (11), such that the

magnon band coincides with the phonon band 2 at the energy $E = 1.2$. Figure 4(d) shows that the magnon and phonon band 2 have a strong coupling; it can be characterized by an obvious band anticrossing at the K' point, but the coupling disappears at the K point. This case is quite similar to the case of $m_A = m_B$ shown in Fig. 4(a). The speculation in terms of P_A^z also applies to this case: Figs. 3(b) and 3(f) show that P_A^z is -1 at the K point but P_A^z is $+1$ at the K' point. So the coupling between magnons and phonons at the K' point and K point is inconsistent.

For the normal modes of phonon band 3 at both the K and K' points, atom A is frozen at its equilibrium position ($C_A = 0$) as shown in Figs. 3(c) and 3(g). The special normal modes provide an opportunity to test our previous speculation based on P_A^z, which states that the magnon only couples with phonon modes with CCW rotations of atom A. As a result, the coupling between the magnon band and these phonon bands is expected to vanish. We set $J = 1.6$, which makes the magnon band coincide with phonon band 3 at $E = 1.35$. The calculated dispersion relation as shown in Fig. 4(e) confirms the absence of magnon-phonon coupling at both the K and K' points.

Finding the band anticrossing feature in the dispersion relation is not a convenient approach for studying the magnon-phonon coupling, especially for magnons and phonons in nonresonant conditions. The coupling strength is the absolute value of off-diagonal elements of the dynamic matrix based on uncoupled phonon and magnon normal modes. The calculated coupling strengths for the cases of $m_A = m_B$ and $m_A \neq m_B$ are shown in Figs. 6(a) and 6(b), respectively; they share some common features. The coupling strength between the magnon band and all phonon bands is zero at the Γ point. This is because the H_c term in the total energy involves the DMI between next-nearest neighbors, i.e., for sublattices i and j, it can be written as $H_c = D_\parallel \sum_{ij} (\vec{u}_{i(k,R)} - \vec{u}_{j(k,R)}) \cdot (\overrightarrow{\delta S}_{i(k,R)} - \overrightarrow{\delta S}_{j(k,R)})$. At the Γ point, one has both $\vec{u}_i = \vec{u}_j$ and $\delta \vec{S}_i - \delta \vec{S}_j = 0$; so the magnon-phonon coupling vanishes $[H_c(\Gamma) = 0]$.
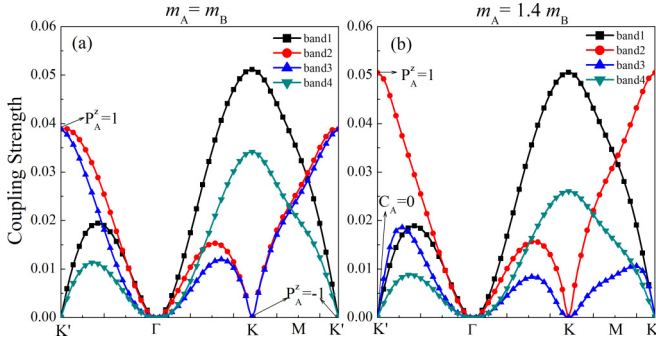
FIG. 6. The magnon-phonon coupling strength on a highly symmetric path with $D_{\parallel} = 0.01$ in the one-magnetic-sublattice system. (a) The coupling strength of the acoustic magnon with four phonon bands at $m_A = m_B$. (b) The coupling strength between the acoustic magnon and the four phonon bands with $m_A = 1.4 \, m_B$. Black squares, phonon band 1; red circles, phonon band 2; blue triangles, phonon band 3; cyan inverted triangles, phonon band 4.
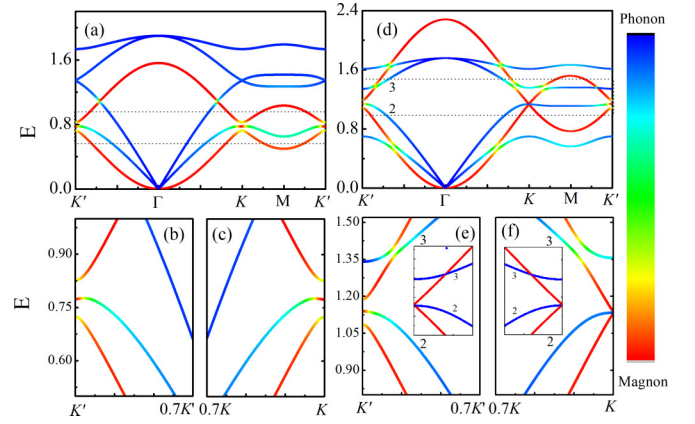

FIG. 7. The magnon-phonon coupling in a FM honeycomb lattice. (a) The magnon-phonon dispersion relation at $m_A = m_B$. (b) Enlarged view near the K' point in (a). (c) Near the K point the enlarged view in (a). (d) The magnon-phonon coupling dispersion relation for chiral phonons with $m_A = 1.4 \, m_B$. (e) and (f) Enlarged views near the K' and K points in (d); the insets show the band without magnon-phonon coupling.

The magnon-phonon coupling strength as a function of phonon angular momentum is shown in Fig. 5. From Eq. (5) we can write the displacement $\vec{u}_{i(k,R)}$ and $\delta S_{j(k,R)}$ in the form of amplitude and polarization. So the coupling term is $H_c \propto D_{\parallel} \cdot C_p D_m \cdot \sum_k \vec{\epsilon}_m^+(k) \cdot \vec{\epsilon}_p(k)$, where C_p and $\epsilon_p(k)$ are the amplitude and polarization of the phonon. D_m and $\epsilon_m(k)$ are the amplitude and polarization of the magnon, and $D_{\parallel}$ is a constant. We suppose that the polarization of the magnon is rotated CCW with $\vec{\epsilon}_m(k) = a\binom{1}{i}$ and the polarization of the phonon is $\vec{\epsilon}_p(k) = a\binom{1}{i} + b\binom{1}{-i}$. Here, $a^2 + b^2 = 1$; according to Eq. (8) we can know that the phonon polarization of sublattice α is $P_\alpha^z = \vec{\epsilon}_\alpha^+ \hat{P} \vec{\epsilon}_\alpha = a^2 - b^2$. So the phonon polarization multiplied by the magnon polarization becomes $\vec{\epsilon}_m^+(k) \cdot \vec{\epsilon}_p(k) \propto 1 + P_\alpha^z$. The coupling strength can be simplified as $H_c \propto C_\alpha D_\alpha \cdot (S_\alpha^z + P_\alpha^z)$. Thus the coupling strength is related to the sublattice amplitude and polarization of the magnon and phonon.

We first look at the case of $m_A = m_B$ as shown in Fig. 6(a). Some phonon modes at high-symmetry points are coupled with the magnon band, e.g., phonon bands 2 and 3 at the K' point, as well as phonon bands 1 and 4 at the K point. These phonon modes possess phonon polarization of $P_A^z = +1$. However, phonon bands 2 and 3 at the K point and phonon bands 1 and 4 at the K' point are decoupled from the magnon band; these phonon modes have $P_A^z = -1$. From the coupling strength $H_c \propto C_\alpha D_\alpha \cdot (S_\alpha^z + P_\alpha^z)$, we can understand the finite or vanishing coupling strength as mentioned above. When $P_A^z + S_A^z = 0$ (with $S_A^z = +1$ and $P_A^z = -1$), the coupling strength vanishes.

The coupling strength difference between the case of $m_A \neq m_B$ and the case of $m_A = m_B$ is the vanishing coupling between the magnon band and phonon band 3 at the K' point, as shown in Fig. 6(b). This phonon mode involves a frozen sublattice A with the displacement amplitude $C_A = 0$. The amplitude of the magnon is $D_A = 1$. So the coupling strength of phonon band 3 is zero at the K' point. The explicit calculations of magnon-phonon coupling strength confirm that the magnon mode on the sublattice A is not coupled with the

phonon modes either with $P_A^z = -1$ or with the displacement amplitude of $C_A = 0$.

2. The case of FM-coupled sublattices

In this section, we consider the case where both sublattices carry local spins and the ground state is ferromagnetic. The antiferromagnetic case will be discussed in the next section. In this case, both sublattices A and B possess local spins as depicted in Fig. 1(b). All the spins align with the $+z$ direction in the ground state with $S_A^z = +1$ and $S_B^z = +1$. There are two magnon bands, namely acoustic and optical bands. The two magnon bands join at both the K and K' points to form a Dirac cone therein.

We first study the case of $m_A = m_B$; the case of different masses will be discussed later. The magnon-phonon dispersion relation calculated along the high-symmetry path in the first Brillouin zone is plotted in Fig. 7(a). The red pseudocolor corresponds to pure magnon states, and blue corresponds to pure phonon states. We focus on the regions near the K and K' points, where degenerate acoustic and optical magnon bands form Dirac cones by themselves. We tune the exchange strength of the magnon [J in Eq. (11)] so that one phonon band coincides with the magnon Dirac cone at $E = 0.75$; the aim is to maximize the anticrossing between magnon and phonon bands. Figures 7(b) and 7(c) zoom out the regions near the magnon Dirac cones. Both magnon bands are repelled by the phonon band, and the magnon Dirac cones disappear at both K and K' points. The pseudocolors of these bands indicate strong coupling between magnons and phonons. Comparing Figs. 7(b) and 7(c), one observes that the splitting of magnon bands at the K' point is identical to that at the K point, indicating that the magnon-phonon coupling at the K point is the same as that at the K' point. This is distinct from the case of having only one magnetic sublattice; see Figs. 4(b) and 4(c). We invoke the phonon polarization to understand the magnon-phonon coupling in this case. As we have learned above, magnons only couple to phonon modes with the same

polarization. For the lower acoustic phonon mode, at the K point, the phonon polarization of sublattice A is $P_A^z = +1$, while that of sublattice B is $P_B^z = -1$. Therefore magnon-phonon coupling occurs within the A sublattice. At the K' point, $P_A^z = -1$ and $P_B^z = +1$, and the magnon-phonon coupling occurs in the B sublattice. More importantly, in both cases, the magnitude of phonon modes on the A sublattice is the same as that on sublattice B. Therefore the strength of magnon-phonon coupling is the same on the K and K' points. The same argument can be applied to the higher optical phonon mode.

The preceding discussion indicates that the magnon-phonon coupling at the K point would be no longer equal to that at the K' point if the symmetry between sublattice A and sublattice B breaks. We set different masses for atoms A and B: $m_A = 1.4\, m_B$ to break the inversion symmetry of the lattice. The calculated magnon-phonon dispersion relation is shown in Figs. 7(d)–7(f). Even if we turn off magnon-phonon coupling, the two phonon bands labeled as bands 2 and 3 in Figs. 7(e) and 7(f) no longer join each other at the K and K' points shown in the insets. The normal mode of phonon band 2 at the K' point involves solely circular motion of sublattice A with $P_A^z = +1$, while sublattice B remains frozen, as shown in Fig. 3. As expected, this phonon mode hybridizes with both magnon modes opening a gap at the magnon Dirac cone; Fig. 7(e) shows the splitting of the three bands between $E = 1.05$ and $E = 1.20$. At the K point, sublattice A solely contributes to the normal mode and has $P_A^z = -1$. As a result, this phonon band fails to hybridize with magnon bands forming the Dirac cone; see Fig. 7(f). We observe a selective coupling between magnon and chiral phonons.

Figures 7(e) and 7(f) show the coupling between phonon band 3 and the optical magnon band. The coincidence of phonon and magnon band energy occurs at about the $0.9K$ and $0.9K'$ points. The anticrossing magnitude proportional to the magnon-phonon coupling strength is larger at $0.9K$ than at $0.9K'$. At these points, the phonon normal modes for each sublattice involve elliptical instead of circular movements. The total phonon angular moment at the $0.9K$ point is positive, while the phonon angular moment is negative at the $0.9K'$ point, which explains the stronger magnon-phonon coupling at the $0.9K$ point.

The calculated magnon-phonon coupling strength between the four phonon bands and the two magnon bands is shown in Fig. 8. The coupling strength is consistent with the dispersion relations displayed in Fig. 7. All the magnon-phonon coupling vanishes at the Γ point, because $\vec{U}_i = \vec{U}_j$ and $\vec{S}_i = \vec{S}_j$ always hold in Eq. (13). For the case of $m_A = m_B$, Figures 8(a) and 8(b) show that the magnon-phonon coupling strength along the Γ-K path is the same as that along the Γ-K' path; the same goes for the M-K and M-K' paths. This phenomenon reflects the symmetry of the lattice in this case. The inversion operation keeps the system unchanged, equivalent to exchanging sublattice A with sublattice B. The inversion operation also exchanges the K point with K', which explains the abovementioned symmetry of the magnon-phonon coupling strength.

In FM-coupled sublattices with $m_A = m_B$, the magnons have equal amplitude and polarization ($D_A = D_B = 1$ and $S_A^z = S_B^z = 1$). This coupling strength is always nonzero at the K and K' points. Taking the K' point as an example, the
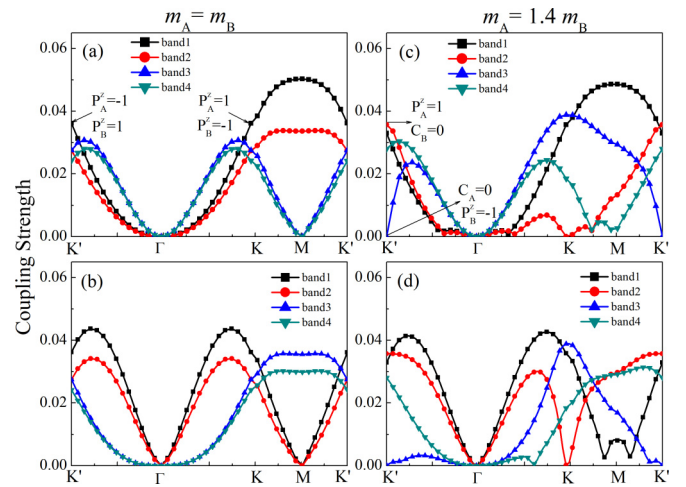

FIG. 8. The strength of magnon-phonon coupling in a FM system with $D_{||} = 0.01$. (a) The coupling strength between the optic magnon and the four phonon bands at $m_A = m_B$. (b) The strength of the acoustic magnon and the phonon on four energy bands at $m_A = m_B$. (c) The optic magnon coupled with the four phonon bands at $m_A = 1.4\, m_B$. (d) The coupling strength between the acoustic magnon and phonons at $m_A = 1.4\, m_B$. Black squares, band 1; red circles, band 2; blue triangles, band 3; cyan inverted triangles, band 4.

polarizations of phonon bands 1 and 4 have $P_A^z = -1$ and $P_B^z = +1$, the term of $(P_A^z + S_A^z)$ is zero, and hence the magnon-phonon coupling of sublattice A vanishes; the coupling between phonons and magnons is conducted by sublattice B. Phonon bands 2 and 3 have $P_A^z = +1$ and $P_B^z = -1$, and similarly, $(P_B^z + S_B^z) = 0$; these phonon modes couple with the magnons via sublattice A.

Figures 8(a) and 8(b) also show that at the M point, the acoustic (optical) magnon modes are not coupled with optical (acoustic) phonon modes. This can be explained by the phase difference between the two sublattices of these normal modes. For acoustic magnon and phonon modes, the phase difference is zero, while optical modes have a phase difference of π.

For the case of $m_A \neq m_B$, the symmetry between K and K' points no longer holds, as shown in Figs. 8(c) and 8(d). The asymmetry can also be understood using the proposed coupling strength H_c. At the K' point, phonon band 2 has $P_A^z = +1$ and $C_B = 0$, which results in $H_c = 2C_A \neq 0$; phonon band 3 has $C_A = 0$ and $P_B^z = -1$, such that $H_c = 0$, and the coupling between phonon band 3 and the magnons disappears. At the K point, in contrast, phonon band 2 has $P_A^z = -1$ and $C_B = 0$, and the coupling strength H_c is zero. Phonon band 3 has $C_A = 0$ and $P_B^z = +1$, which implies that $H_c = 2C_B \neq 0$. Figures 8(c) and 8(d) tell us that both magnon bands are coupled with phonon band 3, but not phonon band 2.

3. The case of AFM-coupled sublattices

Lastly, we discuss the case of AFM-coupled sublattices. At the ground state, the spin on atom A points in the $+z$ direction, while the spin on atom B points in the $-z$ direction. The two magnon modes are degenerate in the absence of external magnetic fields. The normal mode of the magnon at the center of the first Brillouin zone involves the precessions of both
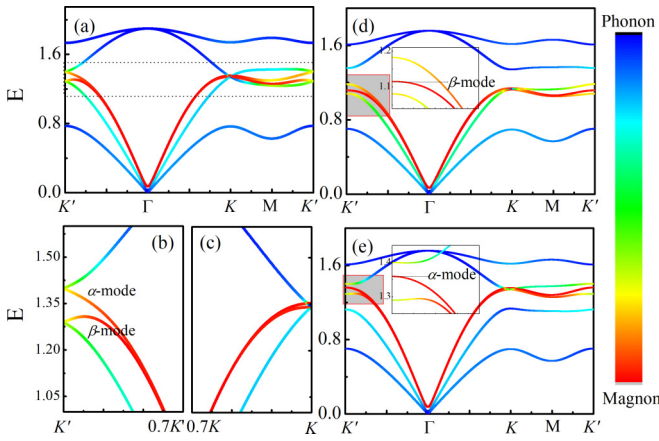
FIG. 9. Hybrid magnon-phonon modes in an AFM system. (a) Energy bands of magnon-phonon coupling with $J = 1.5$ and $m_A = m_B$. (b) Enlarged view near the K' point in (a). (c) Near the K point the enlarged view in (a). (d) The α-magnon mode coupling with the second phonon at $m_A = 1.4 \, m_B$, $J = 1.4$. (e) The β-magnon mode coupling in phonon band 3 with $m_A = 1.4 \, m_B$, $J = 1.6$.

FIG. 10. The strength of magnon-phonon coupling on a highly symmetric path with $D_\| = 0.01$. (a) The coupling strength of the α magnon mode with the four phonon at $m_A = m_B$. (b) The coupling strength between the β magnon mode and the phonons with $m_A = m_B$. (c) The strength of the α magnon mode and phonons with $m_A = 1.4 \, m_B$. (d) With $m_A = 1.4 \, m_B$, the magnon-phonon coupling strength between the β magnon mode and phonons. Black squares, band 1; red circles, band 2; blue triangles, band 3; cyan inverted triangles, band 4.

spins on sublattices around their equilibrium directions. For one of the modes, the precession of spins on sublattice A is along the CCW direction, but spins on sublattice B are along the CW direction, which is called the α mode. The β mode involves spin precession in the opposite direction to that of the α mode. In the linear regime, the deviation of spins is small, and the spins can be described by their transverse components. For the α (β) magnon mode, transverse components of spins on both sublattices rotate in the CCW (CW) direction. This is distinct from the case of FM-coupled sublattices in which the deviations of both spins rotate along the same direction. Figure 9(a) shows the calculated magnon-phonon dispersion relation for the case of $m_A = m_B$. Magnon bands denoted as a red curve in Fig. 9(a) are almost always degenerate, except in the region near the K' point where strong coupling with phonons occurs. The magnon-phonon dispersion relation near the K' point, as depicted in Fig. 9(b), differs from all previously discussed cases. The two magnon modes are no longer degenerate, and the Dirac cone formed by two phonon bands is also gapped out.

The joining and repulsing patterns of these bands may suggest that the optical phonon only couples with one of the magnon modes, while the acoustic phonon couples with the other magnon mode; the uncoupled magnon and phonon modes remain degenerate at the K' point. However, this is not the case, as we discuss later. At the K point as shown in Fig. 9(c), in contrast, there is no sign of band repulsion, which indicates that the couplings between the magnon bands and the two phonon bands vanish.

We also studied the case with $m_A \neq m_B$. Two calculated band structures with different J are shown in Figs. 9(d) and 9(e). In Fig. 9(d), the value of J is delicately tuned such that the magnon bands coincide with the higher acoustic phonon band at the K and K' points. The magnon-phonon coupling is characterized by the band repulsion and the reduction of the magnon component in the normal modes (no longer red in pseudocolor). The β magnon mode is decoupled from the
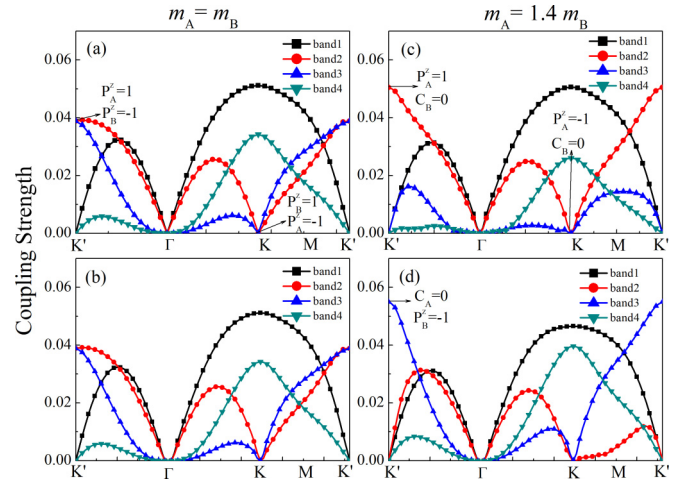
phonon mode since its pseudocolor remains red, while the α magnon mode is coupled with the phonon since its pseudocolor turns yellow, as shown in the inset of Fig. 9(d).

The two magnon modes are not coupled with the phonon at the K point. We also tune the value of J to make the magnon bands join the lower optical phonon bands at the K and K' points. The calculated band structure in Fig. 9(e) shows the same characteristics as in Fig. 9(d): At the K' point, only one magnon is coupled with the phonon, whereas there is no magnon-phonon coupling at the K point. At first sight, the band structure of the $m_A \neq m_B$ case is quite similar to the case of $m_A = m_B$ in band 1 and band 4. However, they are not the same as bands 2 and 3, and we will discuss their differences below.

The calculated magnon-phonon coupling strength between the four phonon bands and two degenerate magnons is shown in Fig. 10. At the Γ point, all the coupling vanishes. From Figs. 10(a) and 10(b), one can observe that at the K point, phonon bands 2 and 3 are decoupled from both magnon bands; this is consistent with the band structure in Fig. 9(c).

At the K' point, the coupling strengths between these two phonon bands and both magnon bands have the same magnitude. This disproves our initial guess that the optical phonon couples with the α magnon mode and the acoustic phonon couples with the β magnon mode. Next, we discuss how to understand the band degeneracy at the K' point in Fig. 9(b). We consider a four-band model of the two magnon modes and two phonon modes; its diagonal elements are the frequencies of magnon and phonon modes in the absence of magnon-phonon coupling. As mentioned before, we deliberately choose the magnetic exchange parameter so as to make the Dirac cone of the magnon coincide with the Dirac cone of the phonon, so the diagonal elements of the four-band model

are the same, denoted as ω. The off-diagonal elements are the coupling strength between magnon and phonon modes. The results in Figs. 10(a) and 10(b) put a constraint on the off-diagonal elements: They shall have the same absolute value (denoted as $g > 0$). The Hamiltonian in the subspace of two magnon modes and two phonon modes can be written as a real symmetric matrix,

$$
\begin{pmatrix}
\omega & 0 & \pm g & \pm g \\
0 & \omega & \pm g & \pm g \\
\pm g & \pm g & \omega & 0 \\
\pm g & \pm g & 0 & \omega
\end{pmatrix}, \tag{14}
$$

where the diagonal elements are the frequencies of noninteracting magnons and phonons: They are the same when the coupling between them is not permitted. The first two columns and rows correspond to the two magnon modes, and the other two correspond to the two phonon modes. The plus and minus signs can be chosen arbitrarily as long as the matrix remains symmetric.

We have tried all the different choices of the plus and minus signs, and we found that when the matrix has a form of

$$
\begin{pmatrix}
\omega & 0 & g & -g \\
0 & \omega & g & -g \\
g & g & \omega & 0 \\
-g & -g & 0 & \omega
\end{pmatrix}
\quad \text{or} \quad
\begin{pmatrix}
\omega & 0 & -g & g \\
0 & \omega & -g & g \\
-g & -g & \omega & 0 \\
g & g & 0 & \omega
\end{pmatrix}, \tag{15}
$$

the calculated eigenfrequencies are $\omega - \sqrt{2}g$ and $\omega + \sqrt{2}g$; both of them are doubly degenerate, consistent with the double degeneracy at the K' points as shown in Fig. 9(b). Next, we explain the strength of the magnon-phonon coupling in the AFM lattice. The normal mode of the AFM magnon is different from that of the FM case. The magnitude of transverse deviations of spins on sublattice A is always equal to that on sublattice B. For the magnon modes in AFM, however, the magnitudes are different on the two sublattices. Hereafter, we use D_γ^z to refer to the magnitude of the magnon on the sublattice γ ($\gamma = A, B$). S_γ^z is the polarization of the magnon.

The magnon modes at the K, K', and M points are shown in Fig. 11. The α magnon mode at the K point is shown in Fig. 11(a). Only the spins on sublattice A rotate CCW corresponding to $S_A^z = +1$, while the spins on sublattice B keep their equilibrium direction with the amplitude equal to zero ($D_A^z = 0$). For the β magnon mode, one has $S_B^z = -1$ and $D_A^z = 0$ according to Fig. 11(b). The magnon modes at the M point [Figs. 11(e) and 11(f)] are an example of general K points. At general K points the α (β) mode corresponds to $S_A^z = S_B^z = +1$ (-1) with finite amplitudes D_A^z and D_B^z.

From Figs. 10(a) and 10(b) one can infer that when $m_A = m_B$, the coupling strength with four phonon bands is the same for α and β magnon modes. At the K' point, phonon bands 1 and 4 are not coupled with any magnon modes, because these phonon modes have $P_A^z = -1$ and $P_B^z = +1$. In contrast, phonon bands 2 and 3 are strongly coupled with both magnon modes; these phonon modes instead have $P_A^z = +1$ and $P_B^z = -1$. We list the characteristics of these magnon and phonon modes in Fig. 11(g) for convenience. Using the data shown in Fig. 11(g), one can calculate the coupling strength for a given magnon mode and phonon mode. For the α magnon mode with $D_A = 1$, $D_B = 0$, and $S_A^z = +1$, the coupling strength is
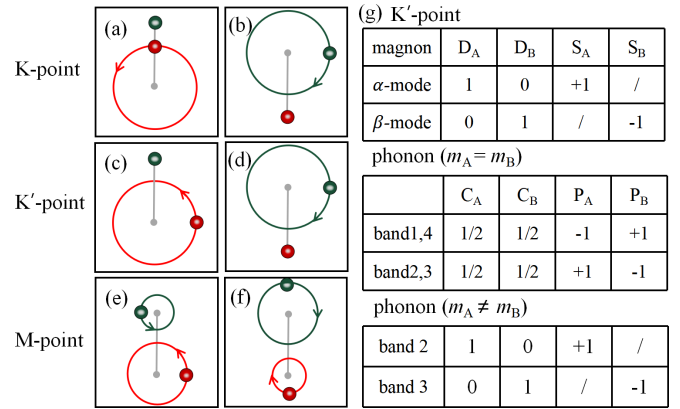

FIG. 11. The two magnon modes in AFM-coupled sublattices. (a) and (b) The α and β magnon modes at the K point. (c) and (d) The two modes at the K' point. (e) and (f) The α and β magnon modes at the M point. (g) The amplitudes and polarizations of magnons and phonons at the K' point.

$(P_A^z + 1)/2$. One can prove that $H_c = 0$ for both phonon mode 1 and phonon mode 4 because they have $P_A^z = -1$. However, $H_c \neq 0$ for phonon modes 2 and 3, because they have $P_A^z = +1$. $H_c = (P_B^z - 1)/2$, for the β magnon mode with $D_A = 0$, $D_B = 1$, and $S_B^z = -1$. Therefore the α magnon mode is not coupled for phonon modes 1 and 4 but has finite coupling for phonon modes 2 and 3.

From the K' point to the K point, the magnon polarizations (S_A^z and S_B^z) and magnon amplitudes (D_A and D_B) remain unchanged; however, the phonon polarizations P_A^z and P_B^z change their signs (see Fig. 2). Therefore this is equivalent to exchanging phonon bands 1 and 4 with phonon bands 2 and 3. So one has $H_c \neq 0$ for phonon bands 1 and 4 at the K point and $H_c = 0$ for phonon bands 2 and 3, which is consistent with the calculated magnon-phonon coupling at the K point.

The calculated magnon-phonon coupling for the case of $m_A \neq m_B$ is shown in Figs. 10(c) and 10(d). Compared with the case of $m_A = m_B$, the only difference occurs at the K' point: The coupling between phonon band 3 and the α magnon vanishes; so does the coupling between phonon band 2 and the β magnon. The α magnon has $D_A = 1$ and $D_B = 0$, while phonon band 3 has $C_A = 0$ and $C_B = 1$; therefore we have the vanishing coupling between them. Notably, the data listed above also mean that the magnon mode and the phonon mode are carried by different sublattices; naturally, they are not coupled. The same analysis can also be applied to the coupling between phonon band 2 and the β magnon.

The curves of coupling strength as shown in Figs. 8 and 10 have distinct behaviors near the Γ point, reflecting that the acoustic (optical) magnons have a stronger coupling with acoustic (optical) phonons than optical (acoustic) phonons. The difference in coupling strength is attributed to the phase difference of normal modes within one primitive unit cell. For the normal modes of acoustic phonon and magnon bands, the phase difference is near zero; while the phase difference is near π for optical magnon and phonon bands. Finally, we analyze what we learn from the magnon-phonon coupling strength. The product $D_\gamma C_\gamma$ with $\gamma = A, B$ appearing in the H_c means that it is possible for a phonon mode to couple

with a magnon mode only when both of them involve the same sublattice. The summation of $P_\gamma^z + S_\gamma^z$ appearing in the expression of H_c means that a magnon with $S^z = +1 \,(-1)$ is not coupled with a phonon $P^z = -1 \,(+1)$. In this sense, the P^z of the phonon and the S^z of the magnon can be interpreted as the angular momentum. Besides the honeycomb lattice, the selective coupling between magnons and chiral phonons also exists in the kagome lattice. The Supplemental Material [43] shows the coupling of magnons with both achiral and chiral phonons in the ferromagnetic kagome lattice.

IV. CONCLUSIONS

In this paper, we have studied the coupling of magnons with chiral phonons in honeycomb lattices. We emphasize the role played by the angular momentum of chiral phonons in determining the magnon-phonon coupling strength. We thoroughly investigated the coupling between two different types of phonons (achiral and chiral) and three types of magnons (magnons living on one sublattice, FM magnons, and AFM magnons). The results reveal that the angular momentum of the phonons regulates the magnon-phonon coupling strength. The method and analysis presented in this paper are also applicable to the first-principles calculation of magnon-phonon coupling strengths in specific materials. The dispersion relation of magnons becomes nonreciprocal, i.e., $\omega(\boldsymbol{k}) \neq \omega(-\boldsymbol{k})$ when coupled with chiral phonons, so the magnon transport also becomes nonreciprocal. At the same time, the phonon dispersion and its transport also exhibit nonreciprocality. For instance, the nonreciprocality in the dispersion relations of magnons and phonons can be tested in

experiments via inelastic neutron scattering. The nonreciprocal magnon has applications in the fields of spintronics and magnonics. The thermal transport properties of materials can be manipulated by nonreciprocal phonons. Both the magnons and chiral phonons have finite angular momentum. The coupling strength between magnons and chiral phonons is controlled by their angular momentum. Based on this principle, one can design chiral materials or heterostructures to exhibit strong magnon-phonon coupling. In addition, the conservation of angular momentum during the interaction between magnons and phonons provides a route to carry the angular momentum of a magnon system by long-lived phonons. The asymmetric magnon-phonon coupling at the K and K' points of a hexagonal lattice is an analog of the valley splitting in electronic systems. The magnon couples with the phonon at one of the high-symmetry points but not the other. The resulting magnon-polarons would occupy only one valley and not the other. If there is a coupling channel between the magnon-polaron and electronic states, the presence of magnon-polarons at one valley would cause valley splitting in the electronic system and lead to the valley Hall effect.

[1] L. Zhang, J. Ren, J.-S. Wang, and B. Li, Phys. Rev. Lett. **105**, 225901 (2010).

[2] L. Zhang, J. Ren, J.-S. Wang, and B. Li, J. Phys.: Condens. Matter **23**, 305402 (2011).

[3] R. Shindou, R. Matsumoto, S. Murakami, and J.-i. Ohe, Phys. Rev. B **87**, 174427 (2013).

[4] K. Shen and G. E. W. Bauer, Phys. Rev. Lett. **115**, 197201 (2015).

[5] A. Kamra, H. Keshtgar, P. Yan, and G. E. W. Bauer, Phys. Rev. B **91**, 104409 (2015).

[6] B. Sheikhi, M. Kargarian, and A. Langari, Phys. Rev. B **104**, 045139 (2021).

[7] S. Park, N. Nagaosa, and B.-J. Yang, Nano Lett. **20**, 2741 (2020).

[8] X. Zhang, Y. Zhang, S. Okamoto, and D. Xiao, Phys. Rev. Lett. **123**, 167202 (2019).

[9] S. Li and S. Okamoto, Phys. Rev. B **106**, 024413 (2022).

[10] H. Kondo and Y. Akagi, Phys. Rev. Res. **4**, 013186 (2022).

[11] R. Takashima, Y. Shiomi, and Y. Motome, Phys. Rev. B **98**, 020401(R) (2018).

[12] D. A. Garanin and E. M. Chudnovsky, Phys. Rev. B **92**, 024421 (2015).

[13] D. A. Garanin and E. M. Chudnovsky, Phys. Rev. B **103**, L100412 (2021).

[14] A. Rückriegel, S. Streib, G. E. W. Bauer, and R. A. Duine, Phys. Rev. B **101**, 104402 (2020).

[15] S. Mankovsky, S. Polesya, H. Lange, M. Weißenhofer, U. Nowak, and H. Ebert, Phys. Rev. Lett. **129**, 067202 (2022).

[16] M. Strungaru, M. O. A. Ellis, S. Ruta, O. Chubykalo-Fesenko, R. F. L. Evans, and R. W. Chantrell, Phys. Rev. B **103**, 024429 (2021).

[17] L. Zhang and Q. Niu, Phys. Rev. Lett. **115**, 115502 (2015).

[18] L. Zhang and Q. Niu, Phys. Rev. Lett. **112**, 085503 (2014).

[19] H. Zhu, J. Yi, M.-Y. Li, J. Xiao, L. Zhang, C.-W. Yang, R. A. Kaindl, L.-J. Li, Y. Wang, and X. Zhang, Science **359**, 579 (2018).

[20] X. Xu, W. Zhang, J. Wang, and L. Zhang, J. Phys.: Condens. Matter **30**, 225401 (2018).

[21] Y. Liu, C.-S. Lian, Y. Li, Y. Xu, and W. Duan, Phys. Rev. Lett. **119**, 255901 (2017).

[22] X. Xu, H. Chen, and L. Zhang, Phys. Rev. B **98**, 134304 (2018).

[23] H. Chen, W. Zhang, Q. Niu, and L. Zhang, 2D Mater. **6**, 012002 (2019).

[24] S. Chen, Q. Wu, C. Mishra, J. Kang, H. Zhang, K. Cho, W. Cai, A. A. Balandin, and R. S. Ruoff, Nat. Mater. **11**, 203 (2012).

[25] G. Kim, A-R. Jang, H. Y. Jeong, Z. Lee, D. J. Kang, and H. S. Shin, Nano Lett. **13**, 1834 (2013).

[26] L. Sheng, D. N. Sheng, and C. S. Ting, Phys. Rev. Lett. **96**, 155901 (2006).

[27] Y. Liu, Y. Xu, S.-C. Zhang, and W. Duan, Phys. Rev. B **96**, 064106 (2017).

[28] Y.-T. Wang, P.-G. Luan, and S. Zhang, New J. Phys. **17**, 073031 (2015).

[29] P. Wang, L. Lu, and K. Bertoldi, Phys. Rev. Lett. **115**, 104302 (2015).

[30] L. M. Nash, D. Kleckner, A. Read, V. Vitelli, A. M. Turner, and W. T. M. Irvine, Proc. Natl. Acad. Sci. USA **112**, 14495 (2015).

[31] T. Nomura, X.-X. Zhang, S. Zherlitsyn, J. Wosnitza, Y. Tokura, N. Nagaosa, and S. Seki, Phys. Rev. Lett. **122**, 145901 (2019).

[32] S. Liu, A. Granados del Águila, D. Bhowmick, C. K. Gan, T. Thu Ha Do, M. A. Prosnikov, D. Sedmidubský, Z. Sofer, P. C. M. Christianen, P. Sengupta, and Q. Xiong, Phys. Rev. Lett. **127**, 097401 (2021).

[33] J. Cui, E. V. Boström, M. Ozerov, F. Wu, Q. Jiang, J.-H. Chu, C. Li, F. Liu, X. Xu, A. Rubio, and Q. Zhang, Nat. Commun. **14**, 3396 (2023).

[34] A. Cong, J. Liu, W. Xue, H. Liu, Y. Liu, and K. Shen, Phys. Rev. B **106**, 214424 (2022).

[35] C. S. Massimiliano Aquino and G. Miano, J. Comput. Phys. **209**, 730 (2005).

[36] S. Zhang and S. S.-L. Zhang, Phys. Rev. Lett. **102**, 086601 (2009).

[37] X.-Y. Chen and Y.-P. Wang, Phys. Rev. B **104**, 155132 (2021).

[38] H. Chen, W. Wu, S. A. Yang, X. Li, and L. Zhang, Phys. Rev. B **100**, 094303 (2019).

[39] T. Moriya, Phys. Rev. **120**, 91 (1960).

[40] A. Fert and P. M. Levy, Phys. Rev. Lett. **44**, 1538 (1980).

[41] A. Fert, V. Cros, and J. Sampaio, Nat. Nanotechnol. **8**, 152 (2013).

[42] C. Kittel, Phys. Rev. **110**, 836 (1958).

[43] See Supplemental Material at http://link.aps.org/supplemental/10.1103/PhysRevB.108.174426 for a discussion of the coupling of magnons with both achiral and chiral phonons in the ferromagnetic kagome lattice.